Investigating Depth Domain Adaptation for Efficient Human Pose Estimation

Angel Martínez-González[*†], Michael Villamizar[*], Olivier Canévet[*] and Jean-Marc Odobez[*†]

[*] Idiap Research Institute, Martigny, Switzerland
{angel.martinez, michael.villamizar, olivier.canevet, odobez}@idiap.ch
[†] École Polytechnique Fédérale de Lausanne (EPFL), Lausanne, Switzerland

Abstract. Convolutional Neural Networks (CNN) are the leading models for human body landmark detection from RGB vision data. However, as such models require high computational load, an alternative is to rely on depth images which, due to their more simple nature, can allow the use of less complex CNNs and hence can lead to a faster detector. As learning CNNs from scratch requires large amounts of labeled data, which are not always available or expensive to obtain, we propose to rely on simulations and synthetic examples to build a large training dataset with precise labels. Nevertheless, the final performance on real data will suffer from the mismatch between the training and test data, also called domain shift between the source and target distributions. Thus in this paper, our main contribution is to investigate the use of unsupervised domain adaptation techniques to fill the gap in performance introduced by these distribution differences. The challenge lies in the important noise differences (not only gaussian noise, but many missing values around body limbs) between synthetic and real data, as well as the fact that we address a regression task rather than a classification one. In addition, we introduce a new public dataset of synthetically generated depth images to cover the cases of multi-person pose estimation. Our experiments show that domain adaptation provides some improvement, but that further network fine-tuning with real annotated data is worth including to supervise the adaptation process. x

Keywords: Human Pose Estimation, Adversarial Learning, Domain Adaptation, Machine Learning.

1 Introduction

Person detection and pose estimation are fundamental tasks for many vision based systems across different types of computer vision domains, e.g. visual surveillance, gaming and social robotics. Estimating the human pose provide the different systems the means for fine-level motion understanding and activity recognition.

Representation based methods, specifically Convolutional Neural Networks (CNN), are the leading algorithms to address the pose estimation task. Very deep CNN models have shown robustness to pose complexity, people occlusion and noisy imaging, providing excellent results. Normally, the deeper is the CNN architecture, the larger are the computational demands. In addition, the learning task needs sufficient amounts of data that span the human pose configuration space to prevent overfiting.

To alleviate these issues, we propose the use of depth imaging for human body pose estimation using CNNs. By using depth images we lower the complexity introduced by variabilities such as color and texture, which result in using lighter CNN architectures capable for real time deployment. Depth images have been proven to provide relevant information for the task of human pose estimation. Moreover, the need of training data can be addressed by depth image synthesis. The obtained benefits are twofold, 1) they are easier to synthesize than natural RGB images, and 2) accurate body part annotations come at no cost. However, our pose estimation task will suffer from the domain shift. That is, synthetic and real images come from different distributions, limiting the CNN's generalization capabilities on real depth images.

The challenge addressed in this paper is to fill the gap in the performance caused by the domain shift provoked by learning from synthetic depth images to deploy on real ones. We investigate unsupervised domain adaptation methods to exploit large datasets of unlabeled depth images with people to boost the performance of a CNN-based body pose regressor learned from synthetic data. Landmark localization imposes a challenge in typical domain adaptation settings where the final task is image classification and domains mainly vary in viewpoint and objects are mainly image-centered. On this line, we address the need of training data by creating a dataset of synthetically generated depth images to cover multi-person pose estimation settings by generating depth images displaying two person instances. We show how data recorded with the same type of depth sensor is meaningful for unsupervised domain adaptation for pose estimation purposes. We finally analyze the limitations of unsupervised domain adaptation by comparing the results of adapted models with those obtained by performing fine-tuning with few annotated images. Our experiments suggest that domain adaptation solely improves the performance, and can be further boosted by fine-tuning on a small sample of labeled images.

In section 2 we present a review of state-of-the-art CNN-based approaches for body pose estimation and domain adaptation. In Section 3, we present the different data we use for learning and testing purposes and our approach for synthesizing images in multi-person scenarios. Section 4 describes the proposed approach for depth domain adaptation for body pose estimation. Experiments and results are described in Section 5. Finally, Section 6 presents our conclusions and future work.

2 State-of-the-art.

State-of-the-art methods for pose estimation in the deep learning literature mainly cover the RGB domain. They mainly address the task relying on the cascade of detectors concept: sequentially stacking detectors to improve and refine body part predictions. Image context is retrieved through different network kernel resolutions [29,12,20,28], or embedding coarse to fine prediction in the network architecture [18,10,2]. Moreover, learning the relationships between pairs of body parts improves the performance [25,3,11,13].

Depth data has proven to be a good source of perceptual information of great importance, specifically for robotics and autonomous systems. Depth images preserve many

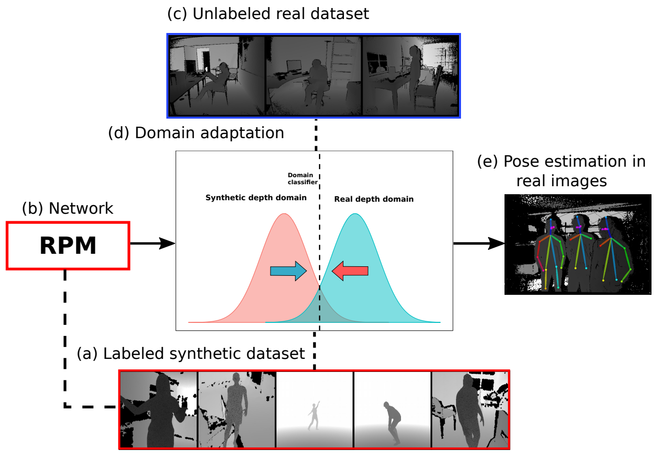

Fig. 1: Scheme of the proposed method for efficient human pose estimation from depth images. A CNN (b) is learned relying on synthetically generated images of people under multiple pose configurations combined with varying real background (a). The domain shift is addressed via an unsupervised domain adaptation method (d) that uses real unlabeled data (c).

essential features that also appear in natural images, e.g. corners, edges, silhouettes, and it is texture and color invariant.

Pose estimation methods from depth images also exist in the CNN literature [9,28,6]. Given that depth image datasets with body part annotations are scarce in the public domain, approaches of this kind use a large network pre-trained on RGB data (e.g. VGG [24]) to fine-tune to the depth domain. However, the use of RGB pre-trained models is not necessarily adequate for the depth domain given the difference between the two data types. In addition, such large pre-trained networks involve many parameters and may unnecessary increase the processing time.

An alternative approach to address the lack of data is via image synthesis [15,23,5,21]. The simplicity of depth images has an advantage for data generation: the lack of texture and color removes some variability factors and simplifies the synthesis process.

A very well known approach that pursued this path is the approach of Shotton et al. [21] proposing a depth image synthesis pipeline to generate a large and varied training set using computer graphics. Still, although a very high realism is achieved, the data does not span the full range of data content. The generated data lacks of typical image characteristics of depth sensors which are difficult to model, as illustrated in Figure 3.

As a result, a model learned and tested on different data origins will suffer a degraded performance provoked by the so called domain shift arising from the differences in visual features. This issue can be alleviated provided extra labeled data for the testing domain. However, since obtaining such data in large enough quantities is often problematic, an unsupervised domain adaptation technique is well suited to learn a predictor in presence of a domain shift between the training (source) and testing (target) data distributions without the need of labeled data in the target domain.

The premise of a domain adaptation technique is to learn a data representation that is invariant across domains. On the one hand, classical machine learning approaches seek to align the data distributions by minimizing the distance between domains provided domain distribution parametrizations [7]. On the other hand, current deep learning methods make use of various training strategies and network architectures to ensure and ease domain confusion and to automatically learn an invariant representation of the data [8,4,16,26,27].

For example [8] proposes to learn invariant data features in a multi-task adversarial setting for object classification. The method learns jointly an object class and domain predictors with shared features among the tasks. Domain adaptation is achieved by an adversarial domain regularizer which aims at fooling the domain classifier, which is in charge of predicting the domain the data comes from. The process encourages the learning of features that makes the domain classifier incapable of distinguish between domains.

Domain adaptation has also been used for the task of 3D pose estimation from RGB images [5]. The approach uses computer graphics software to synthesize colored and textured images of humans that are subsequently merged with natural images as background. Domain adaptation is performed in a two step learning process by alternating the updates of a domain predictor and pose regressor.

Deep domain adaptation in the depth image domain is less covered in the literature. A comparison of state-of-the-art domain adaptation techniques applied to object classification from depth images is presented in [19]. Along the same direction, a method for feature transfer from the real to the synthetic depth domain is presented in [22].

Although deep domain adaptation techniques have obtained remarkable results in transferring domain knowledge, in the majority of the problems the visual domains mainly differ in the objects perspective, lighting, background, and objects are mostly image centered. In addition, most of the final tasks are image classification leaving an open door to apply the same methods for regression problems and object localization tasks, e.g. keypoint detection.

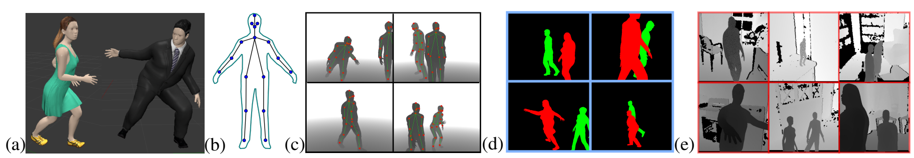

Fig. 2: (a) Examples of the 3D characters we use for depth image synthesis, (b) skeleton model we follow to perform pose estimation, (c) examples of rendered synthetic images, (d) color labeled mask, (e) examples of training images combining synthetic depth silhouettes and real depth background images.

3 Depth Image Domains

This section presents the depth image domains we consider for our pose estimation approach. First, we describe our approach to generate synthetic depth images for multi-person pose estimation settings. Then, we introduce the target data for testing composed of real depth image sequences recorded in a Human-Robot Interaction (HRI) scenario.

3.1 Synthetic Depth Image Generation

Training CNNs requires large amounts of labeled data. Unfortunately, a precise manual annotation of depth images with body parts is troublesome, given that people roughly appear as blobs.

As mentioned before, synthesizing depth images is easier than color images due to the lack of texture, color and lighting. We consider the synthetic depth image database generated by the randomized synthesis pipeline proposed in [17]. The dataset contains images displaying single person instances with different body pose and view perspectives. Yet, it may not be well suited for learning multi-person pose estimation settings like in HRI where people occlusion occur frequently. The data must then reflect these cases. Building upon [17], we improve such pipeline to synthesize depth images displaying two people under different pose configurations, and to extract high quality annotations. The synthesis pipeline is briefly described below.

Variability in body shapes. We consider a dataset of 24 3D characters that show variation in gender, heights and weights, and have been dressed with different clothing outfits to increase shape variation (skirts, coats, pullovers, etc.).

Synthesis with two people instances. We cover the scenarios of multi-person pose estimation by adding two 3D characters to the rendering scene. During synthesis, two models are randomly selected from the character database and placed at a fixed distance between each other. To avoid checking for collision between the characters we set a minimum distance between them during rendering

Variability in body poses. Motion simulation is used to add variability in body pose configurations. We perform motion retargeting from motion capture data sequences taken from the CMU labs Mocap dataset [1].

Variability in view point. A camera is randomly positioned at a maximum distance of 8 meters from the models, and randomly oriented towards the models torso.

Dataset and annotations. The generated image dataset displaying two people instances is publicly available as an extension of the data presented in [17]. Altogether, the two datasets contain 223,342 images of people performing different types of motion under different viewpoints with 51,194 images displaying two people. We automatically extract the location of 17 body landmarks (*head, neck, shoulders, elbows, wrists, hips, knees, ankles, eyes*) in camera and image coordinates. Keypoint visibility labels are also provided. In addition, we extract color labeled silhouette masks for images that contain two people instances. See Figure 2(b) for some examples.

3.2 Real Depth Image Domain Data

Depth imaging is generated as triangulation process in which a series of laser beams are cast into the scene, captured by an infrared camera, and correlated with a reference pattern to produce disparity images and finally the distance to the sensor. The image

(a) (b)
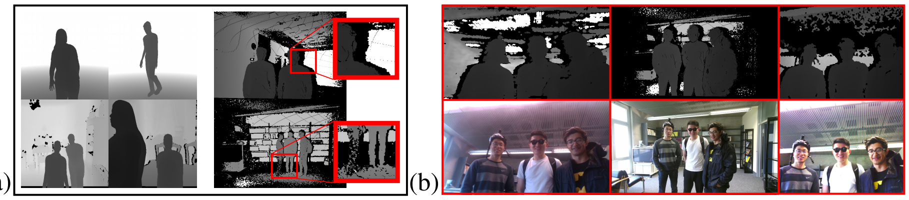

Fig. 3: Depth imaging characteristics. (a) visual characteristics around the human silhouette in depth sensing are difficult to synthesize and therefore not present in the rendered image, (b) HRI scene recorded with different RGB-D cameras, left to right: Intel D435, Kinect 2 and Asus Xtion. Different depth sensors makes the recorded depth images to show specific type of visual characteristics for each sensor.

quality and visual features greatly depend on the sensor specifications, e.g. measurement variance, missing data, surface discontinuities, etc. It is therefore natural to handle depth-based pose estimation learning from synthetic data as a domain adaptation problem, where each depth sensor type constitutes a domain.

We study the problem of depth domain adaptation considering synthetic depth imaging as the source domain and Kinect 2 depth imaging as the target domain. We further focus in HRI settings and consider two datasets.

First, we consider the Watch-n-Patch (WnP) database introduced in [30] which will be used for adaptation purposes. To evaluate the performance of our method, we need a second dataset. To this end, we conducted a series of data collection, recording videos of people interacting with a robotic platform. The recorded data consist of 16 sequences in HRI settings recorded with a Kinect 2. Each of the sequences has a duration of up to three minutes and is composed of pairs of registered color and depth images. The interactions were performed by 9 different participants in indoor settings under different background scene and natural interaction situations. In addition the participants were asked to wear different clothing accessories to add variability in the body shape. Each of the sequences displays up to three people captured at different distance from the sensor. In our experiments we refer to this recorded data as *RLimbs*. Both datasets with annotations, synthetic and recorded HRI sequences, are publicly available [1].

In Section 5 we show how to use this data to bridge the gap between synthetic and real depth image domains, improving the pose estimation performance in real images without the need of annotations on the real data.

4 Depth Domain Adaptation for Pose Estimation

Our pose estimation approach is inspired in the convolutional pose machines (CPM) framework [3]. That is, we predict body parts and limbs of multiple people in a cascade of detectors fashion. In this section we describe the base CNN architecture we follow for pose estimation and the modifications we add to perform depth domain adaptation.

[1] https://www.idiap.ch/dataset/dih

4.1 Base CNN Architecture and Pose Learning

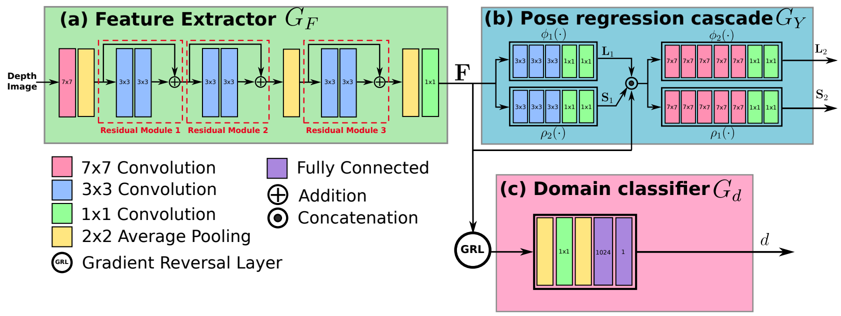

Fig. 4: Architecture design of the CNN used for pose estimation from single channel depth images. The base architecture is composed of a feature extractor module (a), and a pose regression cascade (b). The architecture is further extended with a domain classifier (c) for depth domain adaptation.

Pose Regression CNN Architecture. Figure 4(a) and (b) comprise the base architecture of the pose regression network used to detect body parts and limbs, taking as input a single channel depth image.

Specifically, the neural network architecture is composed of a feature extractor module $G_F(\cdot)$ parametrized by θ_F, and a pose regression cascade module $G_y(\cdot)$ parametrized by θ_Y. For an input depth image $\mathbf{x}$ the feature extractor module computes a compact image representation (features) $\mathbf{F_x} = G_F(\mathbf{x})$ that is internal to the network. This internal image representation $\mathbf{F_x}$ is then passed to the pose regression cascade module $G_Y(\cdot)$ in order to localize body parts and limbs according to our skeleton model (Figure 2(b)).

A predictor t in the pose regression cascade consist on two branches of fully convolutional layers. Branch $\rho_t(\cdot)$ performs the task of body part detection, whereas branch $\phi_t(\cdot)$ localizes body limbs. By considering a number of sequentially stacked detectors, the body parts and limbs predictions are refined using the result of previous stages and incorporating image spatial context through the features $\mathbf{F_x}$.

Finally, pose inference is performed in a greedy bottom-up step to gather parts and limbs belonging to the same person, as originally proposed by the CPM framework.

Feature Extractor Module. The network's feature extraction module $G_F(\cdot)$ computes the image features $\mathbf{F_x}$ by applying a series of residual modules to the image $\mathbf{x}$. The architecture of $G_F(\cdot)$ comprises three residual modules with small kernel sizes and three average pooling layers. Batch normalization and ReLU are included after each convolutional layer and after the shortcut connection.

The architeture of $G_F(\cdot)$ has been designed targeting efficient and fast forward pass, relying on the representational power and efficiency of residual modules. The combination of the processing time taken by the feature extractor together with the cascade of detectors can provide estimations at a frame rate of 35 FPS.

Pose Regression Module. In the pose regression cascade module, each stage t takes as input the image features $\mathbf{F_x}$ and the output of the previous detector $t-1$. As depicted on Figure 4(b), a detector consists of two branches of convolutional layers, the first branch predicting the location of the parts, and the second predicts the location and orientation of the limbs. Note that with only one stage there is no refinement since the first stage only takes as input the features $\mathbf{F_x}$.

Confidence Map Prediction and Pose Regression Loss. We regress confidence maps for the location of the different body parts and predict vector fields for the location and orientation of the body limbs.

The ideal representation of the body part confidence maps $\mathbf{S}^*$ encodes the ground truth location on the depth image as Gaussian peaks. The ideal representation of the limbs $\mathbf{L}^*$ encodes the confidence for the connection between two adjacent body parts, in addition to information about the orientation of the limbs by means of a vector field. We refer the reader to [17] for more details on the generation of the confidence maps.

We define the pair of body parts and body limbs ideal representations as $Y = (\mathbf{S}^*, \mathbf{L}^*)$. Intermediate supervision is applied at the end of each prediction stage to prevent the network from vanishing gradients. This supervision is implemented by two L_2 loss functions, one for each of the two branches, between the predictions $\mathbf{S}_t$ and $\mathbf{L}_t$ and the ideal representations $\mathbf{S}^*$ and $\mathbf{L}^*$. The loss functions at stage t are

$$f_t^1 = \sum_{\mathbf{p} \in \mathbf{I}} ||\mathbf{S}_t(\mathbf{p}) - \mathbf{S}^*(\mathbf{p})||_2^2, \qquad f_t^2 = \sum_{\mathbf{p} \in \mathbf{I}} ||\mathbf{L}_t(\mathbf{p}) - \mathbf{L}^*(\mathbf{p})||_2^2. \tag{1}$$

The pose regression loss is computed as $\mathscr{L}_Y = \sum_{t=1}^{T} \left(f_t^1 + f_t^2\right)$ where T is the total number of stages in the pose regression cascade.

4.2 Depth Domain Adaptation

Ideally, testing and training depth images should live in the same domain. In our case, learning a pose regression network from synthetic data limits its generalization capacity given the missing real depth image details not present in the synthetic training set. We perform domain adaptation to map synthetic and real images to a representation that is similar across domains. We follow closely the method presented in [8] for domain adaptation and adapt it to our body part localization setting.

For our unsupervised domain adaptation learning algorithm we are given a source distribution sample (synthetic depth image dataset) $S = \{(\mathbf{x}_i, \mathbf{y}_i)\}_{i=1}^N \sim \mathscr{D}_S$ and a target dataset sample (real depth image dataset) $T = \{\mathbf{x}_i\}_{i=1}^M \sim \mathscr{D}_T$. We are only given annotations of 2D keypoint locations $\mathbf{y}_i$ for the source distribution samples $\mathbf{x}_i$.

The distance between the source and target distributions can be measure via the H-divergence [8]. Although this is impractical to compute, it can be approximated by the generalization error of the problem of domain classification. In essence, the distance between distributions is minimum if the domain classifier is incapable of distinguishing between the different domains. Therefore, to achieve domain confusion, the data need to be mapped to a representation that is invariant, or at least indistinguishable, across domains.

Let $\mathbf{F_x}$ be the internal representation of image $\mathbf{x}$ in the network (features) computed as $\mathbf{F_x} = G_F(\mathbf{x})$ for a feature extractor $G_F(\cdot)$. A measure of domain adaptation is computed by

$$L_d = -\frac{1}{|S|}\sum_{\mathbf{x}\in S} l_d(G_d(\mathbf{F_x})) - \frac{1}{|T|}\sum_{\mathbf{x}\in T} l_d(G_d(\mathbf{F_x})), \tag{2}$$

where and l_d is a logistic regression loss, and G_d is a domain classifier, parametrized by θ_d, such that $G_d(F_\mathbf{x}) = 1$ if $\mathbf{x} \in T$ and 0 otherwise.

In the problem of domain classification, the domain classifier $G_d(\cdot)$ is fooled when $G_F(\cdot)$ produces equivalent features for both domains. A feature extractor capable of producing such type of features is learned by maximizing Eq (2)

$$R_d = \max_{\theta_d} L_d. \tag{3}$$

Eq (3) aims to approximate the empirical H- divergence between domains S and T as $2(1-R_d)$.

4.3 Joint Pose Learning and Adaptation

The pose learning and domain adaptation joint optimization objective can be written as

$$\mathscr{L} = \mathscr{L}_Y + \lambda R_d, \tag{4}$$

where λ is a parameter that tunes the trade-off between the pose learning and domain adaptation. The second term of Eq (4) acts as a domain regularizer.

Our pose regression network shown in Figure 4(a) and (b) naturally provides the scheme for the joint learning and adaptation problem via a domain classifier (Figure 4(c)). We implement the domain classifier via a neural network composed of two average pooling layers with an intermediate layer of 1×1 convolution and followed by two fully connected layers that produces a sigmoid function. As shown in Figure 4 both the pose regression cascade $G_Y(\cdot)$ and the domain classifier $G_d(\cdot)$ receive as input the features generated by $G_F(\cdot)$.

The learning and adaptation problem stated by Eq (4) proposes an adversarial learning process which involves a minimization with respect to the pose regression loss $\mathscr{L}_Y$ and a maximization with respect to the domain classifier regularizer R_d. We follow [8] by including a gradient reversal layer (GRL) in the architecture to facilitate the joint optimization. The GRL acts as identity function during the forward pass of the network, but reverses the direction of the gradients from the domain classifier during backpropagation.

The nature of pose regression and domain adaptation problems makes the losess involved in Eq (4) to live in different ranges. Therefore, the trade-off parameter λ has to reflect both the importance of the domain classification regularizer as well as to this difference between ranges.

5 Experiments and Results

In a series of experiments we show how different datasets, recorded with the same type of sensor, are used to improve pose estimation via unsupervised domain adaptation. In this section we analyze the performance obtained under different modeling selections on the network architecture and domain adaptation configurations.

5.1 Data

Synthetic domain data. We split the synthetic dataset into three folds with the following percentage and amount of images: training (85%, 189,844), validation (5%, 11,165), and testing (10%, 22,333).

Synthetic training data augmentation. We add the following perturbations to the synthetic images to add realism and avoid overfitting to synthetic clean details.

Adding real background content. We consider the dataset in [14] containing 1,367 real depth images recorded with a Kinect 1 and exhibiting depth indoor clutter. During learning, training images were produced on the fly by randomly selecting one depth image background and body synthetic images, and composing a depth image with background using the character silhouette mask. Sample results are shown in Figure 2(d).

Pixel noise. We randomly select 20% of the body silhouette's pixels and set their value to zero.

Image rotation. Training images are rotated with a probability 0.1 by a randomly selected angle in the range $[-20, 20]$ degrees.

Real domain data. Our real domain consist Kinect 2 data. We use the data presented in Section 3.2 to perform domain adaptation. The Watch-n-Patch dataset was used for adaptation purposes only. We randomly select 85% out of the total number of images comprised over all the sequences, leading to a total of 66,303 depth.

We used the RLimbs data for training, validation and testing purposes. We divide the data taking into account clothing features, actor ID and interaction scenario, in such a way that an actor does not appear in the training and testing sets under similar circumstances. The train, validation and test folds consist of 7, 5 and 4 sequences respectively. We annotate small sets from each fold to be used for validation (750 images), testing (1000 images) and fine-tuning (1750 images).

5.2 Evaluation protocol

Accuracy metric. We use standard precision and recall measures derived from the Percentage of Correct Keypoints (PCKh) as performance metrics [31]. More precisely, we extract landmark predictions p whose confidence is larger than a threshold τ. Pose estimates are generated from these predictions by the part association algorithm. Then, for each landmark type we associate the closest prediction p whose distance to ground truth q is below a distance threshold $d = \kappa \times h$, where h stands for the height of the ground truth bounding box of the person to which q belongs to. The associated predictions p count as true positives and the rest as false positives. Ground truth points q with no associated prediction are counted as false negatives. The average recall and precision values can then be computed by averaging over the landmark types and then over the dataset. Finally, the average recall and precision values used to report performance are computed by averaging the above recall and precision over several distance thresholds by varying κ in the range $[0.05, 0.15]$.

5.3 Implementation details

Pose regression network We use Pytorch as the deep learning framework in all our experiments. First, we train our pose regression network (Figure 4(a) and (b)) on synthetic data with stochastic gradient descent with momentum during 300 K iterations. We set the momentum to 0.9, the weight decay constant to 5×10^{-4}, and the batch size to 10. We uniformly sample values in the range $[4 \times 10^{-10}, 4 \times 10^{-5}]$ as starting learning rate and decrease it by a factor of 10 when the validation loss has settled. All networks are trained from scratch and progressively, i.e. to train network architectures with t stages, we initialize the network with the parameters of the trained network with $t-1$ stages. We consider network architectures with pose regression cascade modules comprised by upto 2 prediction stages.

Domain adaptation. After training the pose regression network for some time with synthetic data, we run the domain adaptation process. The adaptation is performed for $T = 100\ K$ iterations. We monitor and select models according to the lowest value of a validation loss computed on the RLimbs validation set. The learning rate parameter is kept fixed to the last value in the previous training procedure. Domain classifier parameters are randomly initialized using a Gaussian distribution with mean zero and small variance.

We opt to gradually adapt the trade-off parameter λ of eq (4) according to the training progress as

$$\lambda_p = \frac{2\Lambda}{1 + exp(-10p)} - \Lambda, \tag{5}$$

where $p = t/T$ for the current iteration progress t. The constant Λ was experimentally chosen in order to accommodate both losses in eq (4) in the same range. In our experiments we observed a good behavior of pose learning and adaptation for $\Lambda = 100$.

Model notation. We analyze CNN architectures with 1 and 2 prediction stages in the pose regressor cascade. In our results we refer to this configurations as RPM1S and RPM2S respectively. Postfixes -DA and -FT are added whenever used domain adaptation or fine-tuning respectively.

5.4 Results

Domain Adaptation and Network Configuration. We analyze the impact of domain adaptation on the different levels of prediction stages. For these experiments we consider the Watch-n-Patch data for the adaptation process and the RLimbs data for testing. The models were trained as follows. First, a single stage network was trained with synthetic data and then with domain adaptation. Next, a network architecture with 2 stages

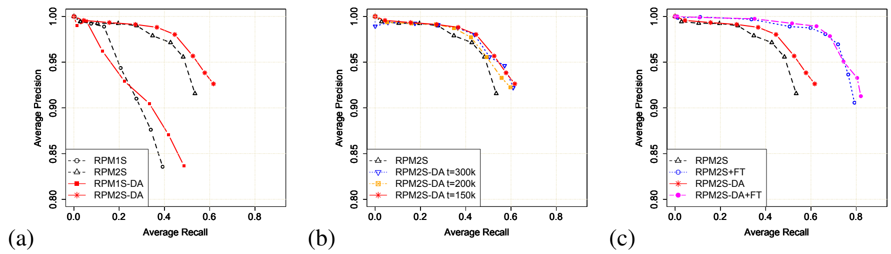

Fig. 5: Average recall-precision curves. (a) impact when applying domain adaptation at the different levels of prediction stages. (b) performance for different starting points of domain adaptation. (c) comparison of domain adaptation and fine-tuning.

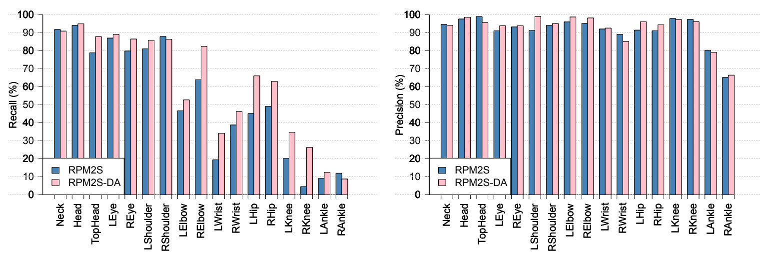

Fig. 6: Recall (left) and precision (right) per body part before and after domain adaptation. Note the high gain in recall for lower body parts after applying domain adaptation.

was trained on synthetic data taking the single stage adapted network as initial point. Finally domain adaptation is performed.

The resultant average recall-precision curves are presented in Figure 5(a). We observe that domain adaptation improves mainly the recall performance at the two levels of prediction stages. Including spatial context via a second prediction stage is vital. Table 1 summarizes these results reporting the models with the largest F1-Score in the curves. The table also shows the performance on the upper-body. In Figure 6 we show a comparison of the per body part precision and recall before and after adaptation. Domain adaptation mainly improves the recall on the lower body parts. As depicted in Figure 3, these parts are the main components in the body silhouettes affected by noise and sensing failures.

Domain Adaptation Starting Point. We conducted experiments in order to find the best training point to start the domain adaptation process. To this end, we start domain adaptation at different points of the synthetic training progress for the RPM2S model. We selected starting points at $t = 150K$, $t = 200K$ and $t = 300K$ training iterations. Figure 5(b) shows the performance of the different learned models. We note the performance among the different runs remains the same. However, the earliest starting point considered show more stable behavior.

	Performance			
	All body		Upper body	
Architecture	AP	AR	AP	AR
RPM1S	83.55	39.20	85.98	55.86
RPM1S-DA	83.68	48.56	89.39	68.63
RPM2S	91.56	53.47	93.93	69.93
RPM2S-DA	**92.62**	**61.66**	**95.00**	**76.09**

Table 1: Comparison of the performance (%) on the RLimbs test set for architectures with different number of prediction stages before and after domain adaptation.

RLimbs based Domain Adaptation. As mentioned before, it is natural to think a depth sensor as a generating domain. We perform domain adaptation using the training fold of the RLimbs database as the target domain sample. As before, we start domain adaptation at different points of the synthetic training and report the model results with the best F1-Score. Table 2 compares the obtained performances. In the table we specifically show the dataset used as target sample during the adaptation process, the source data and the testing data. Note that using both Kinect 2 datasets in the adaptation process improves the performance. Adaptation with the Watch-n-Patch dataset provides slightly better results. It is worth to notice that the number of recorded scenarios, people, and view points contained in the Watch-n-Patch is larger than those contained the RLimbs dataset. This variability is somehow useful in the adaptation process. We include the performance obtained by preprocessing the image with a simple in-paint process. This technique was previously used to alleviate the discontinuities inherited from depth sensing for non adapted models [17]. However, this lowers the precision score with a very little gain in accuracy.

Fine-Tunning. To understand the limits of adapting between depth domains, we performed fine-tunning on an annotated subset of the RLimbs dataset. We considered both, the models trained with synthetic data and adapted models. Figure 5(c) shows the detailed recall- precision curves. As expected, fine tuning on the target data provides better generalization capabilities. However, fine-tuning on models with previous adaptation show further improvement. Table 2 summarizes the results for the models with the largest F1-Score. Figure 7 shows a qualitative comparison of the pose estimation approach for adapted and not adapted models.

6 Conclusions

In this paper we investigated the use of unsupervised domain adaptation techniques applied to the problem of depth-based pose estimation with CNNs. Specifically, we investigated an adversarial domain adaptation method to improve the performance on real depth images of a CNN-based human pose regressor trained with synthetic data. We introduced a new dataset of synthetically generated depth images displaying two people instances to cover cases of multi-person pose estimation. In addition, we presented a

Data			Performance			
			All body		Upper body	
Source	Target	Testing	AP	AR	AP	AR
Synthetic	—	RLimbs	91.56	53.47	93.93	69.93
Synthetic	—	RLimbs (IP)	81.98	58.23	85.20	72.66
Synthetic	WnP [30]	RLimbs	**92.62**	**61.66**	95.00	**76.09**
Synthetic	RLimbs	RLimbs	92.32	59.32	**95.05**	74.55
Synthetic + FT	—	RLimbs	90.56	79.23	93.64	89.52
Synthetic + FT	WnP [30]	RLimbs	**91.27**	**82.03**	93.73	**90.83**
Synthetic + FT	RLimbs	RLimbs	91.03	78.98	**94.32**	89.32

Table 2: Top: comparison of performance (%) by using two different datasets of depth images as the target data for domain adaptation. IP stans for in-paint preprocessing. Bottom: performance obtained by fine tuning (FT) on an annotated subset of the RLimbs training set after learning with synthetic data and after domain adaptation on the different depth image datasets.

dataset containing videos of people in HRI scenarios. Both synthetic and real recorded data are publicly available.

Our experiments show that different data from the same type of sensor is meaningful to cover part of the performance gap introduced by learning from synthetic depth images. However, devoting some effort to label a few examples maybe critical to increase the model's generalization capabilities. We observed that the combination of both approaches, domain adaptation and fine tuning, increase performance. Suggesting that domain adaptation for body pose estimation from depth images a better path to follow is a semi-supervised approach.

ACKNOWLEDGMENTS

This work was supported by the European Union under the EU Horizon 2020 Research and Innovation Action MuMMER (MultiModal Mall Entertainment Robot), project ID 688147, as well as the Mexican National Council for Science and Tecnology (CONACYT) under the PhD scholarships program.

References

1. Cmu motion capture data. http://mocap.cs.cmu.edu/.
2. Adrian Bulat and Georgios Tzimiropoulos. Human pose estimation via convolutional part heatmap regression. In *ECCV*, 2016.
3. Zhe Cao, Tomas Simon, Shih-En Wei, and Yaser Sheikh. Realtime multi-person 2d pose estimation using part affinity fields. In *CVPR*, 2017.
4. Fabio Maria Carlucci, Lorenzo Porzi, Barbara Caputo, Elisa Ricci, and Samuel Rota Bulo. Autodial: Automatic domain alignment layers. In *International Conference on Computer Vision (ICCV)*, 2017.

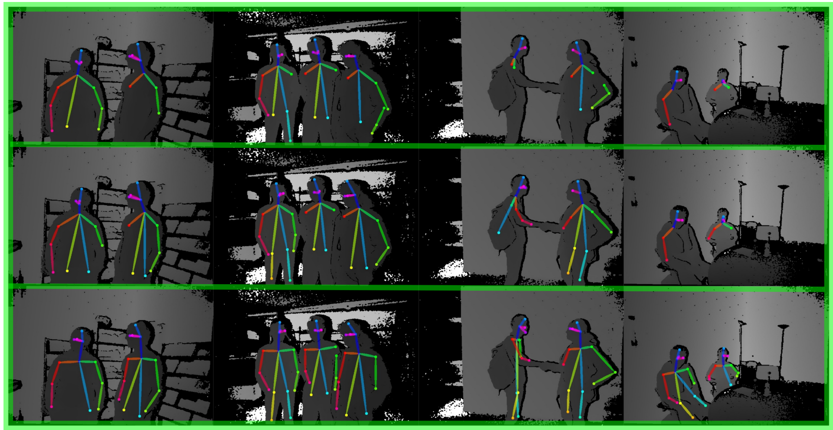

Fig. 7: Output of the different models for some images contained in the testing set of RLimbs. Top row: pose estimation before domain adaptation. Middle row: pose estimation after domain adaptation. Bottom row: pose estimation with fine tuning after domain adaptation.

5. Wenzheng Chen, Huan Wang, Yangyan Li, Hao Su, Zhenhua Wang, Changhe Tu, Dani Lischinski, Daniel Cohen-Or, and Baoquan Chen. Synthesizing training images for boosting human 3d pose estimation. In *3D Vision (3DV)*, 2016.
6. Ben Crabbe, Adeline Paiement, Sion Hannuna, and Majid Mirmehdi. Skeleton-free body pose estimation from depth images for movement analysis. In *IEEE Conference on Computer Vision and Pattern Recognition (CVPR)*, pages 312–320, 12 2015.
7. Gabriela Csurka. Domain adaptation for visual applications: A comprehensive survey. In *Domain Adaptation in Computer Vision Applications*, chapter 1, pages 1–35. Springer Series: Advances in Computer Vision and Pattern Recognition, 2017.
8. Yaroslav Ganin, Evgeniya Ustinova, Hana Ajakan, Pascal Germain, Hugo Larochelle, François Laviolette, Mario Marchand, and Victor Lempitsky. Domain-adversarial training of neural networks. *J. Mach. Learn. Res.*, 17(1):2096–2030, January 2016.
9. Albert Haque, Boya Peng, Zelun Luo, Alexandre Alahi, Serena Yeung, and Li Fei-Fei. Towards viewpoint invariant 3d human pose estimation. In *European Conference on Computer Vision (ECCV)*, October 2016.
10. Peiyun Hu and Deva Ramanan. Bottom-up and top-down reasoning with hierarchical rectified gaussians. In *Proceedings of the 2016 IEEE Conference on Computer Vision and Pattern Recognition*, pages 5600–5609, 06 2016.
11. Eldar Insafutdinov, Mykhaylo Andriluka, Leonid Pishchulin, Siyu Tang, Evgeny Levinkov, Bjoern Andres, and Bernt Schiele. Articulated multi-person tracking in the wild. In *CVPR*, 2017. Oral.
12. Eldar Insafutdinov, Leonid Pishchulin, Bjoern Andres, Mykhaylo Andriluka, and Bernt Schieke. Deepercut: A deeper, stronger, and faster multi-person pose estimation model. In *European Conference on Computer Vision (ECCV)*, 2016.
13. Umar Iqbal, Anton Milan, and Juergen Gall. Posetrack: Joint multi-person pose estimation and tracking. In *IEEE Conference on Computer Vision and Pattern Recognition (CVPR)*, 2017.
14. Kourosh Khoshelham and Er Oude Elberink. Accuracy and resolution of kinect depth data for indoor mapping applications. In *Sensors 2012, 12, 14371454. 2013*, page 8238, 2013.

15. Christoph Lassner, Javier Romero, Martin Kiefel, Federica Bogo, Michael J. Black, and Peter V. Gehler. Unite the people: Closing the loop between 3d and 2d human representations. In *The IEEE Conference on Computer Vision and Pattern Recognition (CVPR)*, July 2017.
16. Mingsheng Long, Han Zhu, Jianmin Wang, and Michael I Jordan. Unsupervised Domain Adaptation with Residual Transfer Networks. In D. D. Lee, M. Sugiyama, U. V. Luxburg, I. Guyon, and R. Garnett, editors, *Advances in Neural Information Processing Systems 29*, page 136144. Curran Associates, Inc., 2016.
17. Angel Martínez-González, Michael Villamizar, Olivier Canévet, and Jean-Marc Odobez. Real-time convolutional networks for depth-based human pose estimation. In *2018 IEEE/RSJ International Conference on Intelligent Robots and Systems, IROS 2018*, 2018.
18. Alejandro Newell, Kaiyu Yang, and Jia Deng. *Stacked Hourglass Networks for Human Pose Estimation*, pages 483–499. Springer International Publishing, Cham, 2016.
19. Novi Patricia, Fabio M. Cariucci, and Barbara Caputo. Deep depth domain adaptation: A case study. In *2017 IEEE International Conference on Computer Vision Workshops, ICCV Workshops 2017, Venice, Italy, October 22-29, 2017*, pages 2645–2650, 2017.
20. Leonid Pishchulin, Eldar Insafutdinov, Siyu Tang, Bjoern Andres, Mykhaylo Andriluka, Peter Gehler, and Bernt Schiele. Deepcut: Joint subset partition and labeling for multi person pose estimation. In *IEEE Conference on Computer Vision and Pattern Recognition (CVPR)*, 2016.
21. J. Shotton, A. Fitzgibbon, M. Cook, T. Sharp, M. Finocchio, R. Moore, A. Kipman, and A. Blake. Real-time human pose recognition in parts from single depth images. In *Proceedings of the 2011 IEEE Conference on Computer Vision and Pattern Recognition*, CVPR '11, pages 1297–1304, Washington, DC, USA, 2011. IEEE Computer Society.
22. Ashish Shrivastava, Tomas Pfister, Oncel Tuzel, Josh Susskind, Wenda Wang, and Russ Webb. Learning from simulated and unsupervised images through adversarial training. In *IEEE Conference on Vision and Pattern Recognition, CVPR*, 2017.
23. Chenyang Si, Wei Wang, Liang Wang, and Tieniu Tan. Multistage adversarial losses for pose-based human image synthesis. In *The IEEE Conference on Computer Vision and Pattern Recognition (CVPR)*, June 2018.
24. Karen Simonyan and Andrew Zisserman. Very deep convolutional networks for large-scale image recognition. 2014.
25. Jonathan J Tompson, Arjun Jain, Yann LeCun, and Christoph Bregler. Joint training of a convolutional network and a graphical model for human pose estimation. In Z. Ghahramani, M. Welling, C. Cortes, N. D. Lawrence, and K. Q. Weinberger, editors, *Advances in Neural Information Processing Systems 27*, pages 1799–1807. Curran Associates, Inc., 2014.
26. Eric Tzeng, Judy Hoffman, Trevor Darrell, and Kate Saenko. Simultaneous Deep Transfer Across Domains and Tasks. In *International Conference in Computer Vision (ICCV)*, 2015.
27. Eric Tzeng, Judy Hoffman, Trevor Darrell, and Kate Saenko. Adversarial Discriminative Domain Adaptation. In *Computer Vision and Pattern Recognition (CVPR)*, 2017.
28. Keze Wang, Shengfu Zhai, Hui Cheng, Xiaodan Liang, and Liang Lin. Human pose estimation from depth images via inference embedded multi-task learning. In *Proceedings of the 2016 ACM on Multimedia Conference*, MM '16, pages 1227–1236, New York, NY, USA, 2016. ACM.
29. Shih-En Wei, Varun Ramakrishna, Takeo Kanade, and Yaser Sheikh. Convolutional pose machines. In *CVPR*, 2016.
30. Chenxia Wu, Jiemi Zhang, Silvio Savarese, and Ashutosh Saxena. Watch-n-patch: Unsupervised understanding of actions and relations. In *The IEEE Conference on Computer Vision and Pattern Recognition (CVPR)*, June 2015.
31. Yi Yang and Deva Ramanan. Articulated human detection with flexible mixtures of parts. *IEEE Trans. Pattern Anal. Mach. Intell.*, 35(12):2878–2890, December 2013.